substance: $FeSi_2$
property: transport properties

resistivity, Hall effect, thermoelectric power and thermal conductivity of pure and Mn-, Co- and Al-doped samples: Figs. 1...17.

absolute thermoelectric power in the intrinsic range

S	$(k/e)[(620/T) - 0.00084]$		polycrystalline samples, annealed at 1173 K, $R_H < 1$ cm^3 C^{-1}	64W

According to [68B], however, $S(T)$ does not follow a T^{-1}-law as the mobility ratio b depends strongly on temperature.

mobilities of charge carriers

(see Fig. 18)

μ_n	0.26 cm^2/V s	T = 300 K	assuming small polarons in n-type $FeSi_2$ (activation energy of the mobility 0.06 eV)	68B
μ_p	2...4 cm^2/V s	T = 300 K	$\mu_p \propto T^{1/2}$ in the extrinsic range	68B
$\mu_p + \mu_n$	1 cm^2/V s	T = 1210 K		69B

mobility ratio

b	0.8	T = 600...850 K	from $S(T)$ (Fig. 7) assuming a simple 2-band semiconductor in the intrinsic range	64W
	0.33	T = 1260 K	(the decomposition temperature of $FeSi_2$)	73N

free-carrier contribution to the thermal conductivity: Fig. 16. Doping with Co and Ni produces n-type material, whereas doping with Mn or substitution of a Group III element for Si leads to p-type material [64W, 73N].

Optimum properties for thermoelectric generators were obtained with Co for n-type doping and Al for p-type doping [64W].

References:

64W Ware, R. M., Mc Neill, D. J.: Proc. IEE 111 (1964) 178.

68B Birkholz, U., Schelm, J.: Phys. Status Solidi 27 (1968) 413.

69B Birkholz, U., Scheim, J.: Phys. Status Solidi 34 (1969) K177.

70B Birkholz, U., Frühauf, A., Schelm, J.: Proc. Tenth Int. Conf. Phys. Semicond., Cambridge, Mass. (1970) 311.

73N Nishida, I.: Phys. Rev. B17 (1973) 2710.

73W Waldecker, G., Meinhold, H., Birkholz, U.: Phys. Status Solidi (a) 15 (1973) 143.

Fig. 1.

$Fe_{1-x}Co_xSi_2$ and $FeSi_{2-y}Al_y$. Resistivity vs. reciprocal temperature [64W]. Samples quenched from the liquid state and annealed at 1173 K. *1*: x = y = 0, *2*: x = 0.005, *3*: x = 0.01, *4*: x = 0.02, *5*: x = 0.03, *6*: x = 0.04, *7*: y = 0.02, *8*: y = 0.04, *9*: y = 0.08.

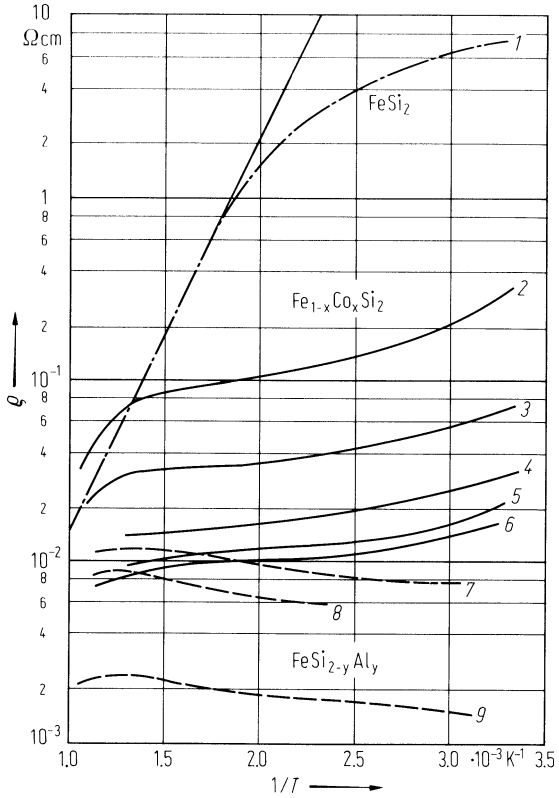

Fig. 2.

$Fe_{1-x}Co_xSi_2$. Conductivity vs. reciprocal temperature [68B]. Samples prepared by sintering at 1453 K and annealing at 1153 K. All samples n-type. Co concentration (in parentheses) in 10^{20} cm^{-3}. *1*: x = y = 0, *2*: x = 0.001, *3*: x = 0.0028, *4*: x = 0.005 (1.31), *5*: x = 0.01 (2.63), *6*: x = 0.029 (7.6), *7*: x = 0.060 (15.8).

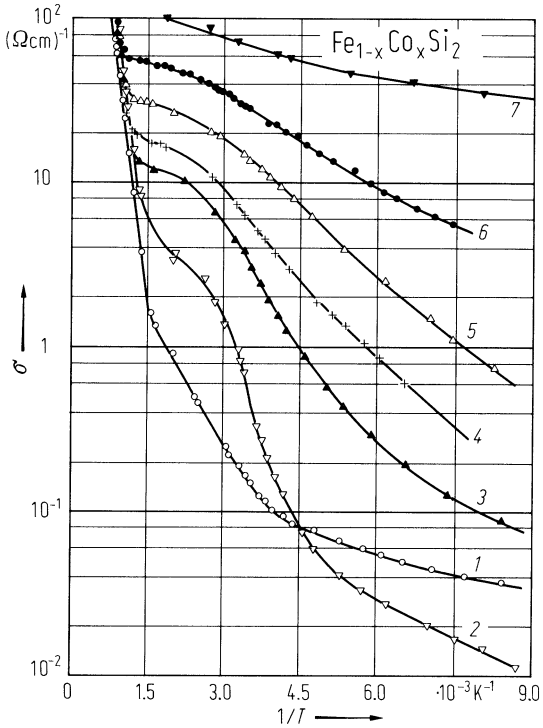

Fig. 3.

$FeSi_{2-y}Al_y$. Conductivity (curves *1*, *2*, *3*) and Hall coefficient (curve *1*') vs. reciprocal temperature [68B]. Al samples p-type; prepared by sintering at 1453 K and annealing at 1153 K *1*, *1*': y = 0.04 ($1.04 \cdot 10^{21}$ Al atoms/cm^3), *2*':y = 0.08 ($2.08 \cdot 10^{21}$ Al atoms/cm^3), *3*: y = 0.08.

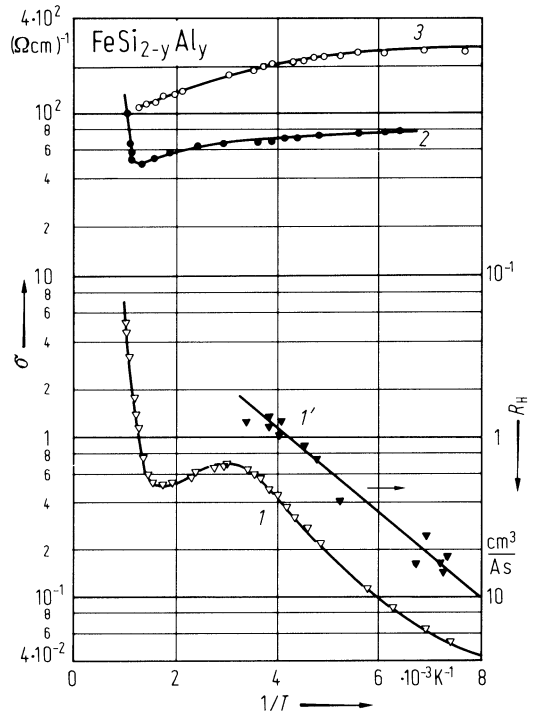

Fig. 4.

$Fe_{1-x}Mn_xSi_2$ and $Fe_{0.95}Co_{0.05}Si_2$. Resistivity vs. reciprocal temperature [73N]. The heating and cooling transition directions are indicated by arrows. *1*: $FeSi_2$ (n-type), *2*: $Fe_{0.97}Mn_{0.03}Si_2$ (p-type), *3*: $Fe_{0.94}Mn_{0.06}Si_2$ (p-type), *4*: $Fe_{0.95}Co_{0.05}Si_2$ (n-type), *5*: metastable inhomogeneous phase. The samples were prepared by hot-pressing at 1423 K and annealing at 1073 K. Curve *5* was measured after quenching the samples from 1400 K. These metastable and inhomogeneous samples were composed of cubic FeSi and tetragonal $Fe_{\approx 0.8}Si_2$ (incorrectly named α-$FeSi_2$, as if it represented the high-temperature modification of orthorhombic "β-$FeSi_2$". Obviously the transformation back to $FeSi_2$ is rather fast).

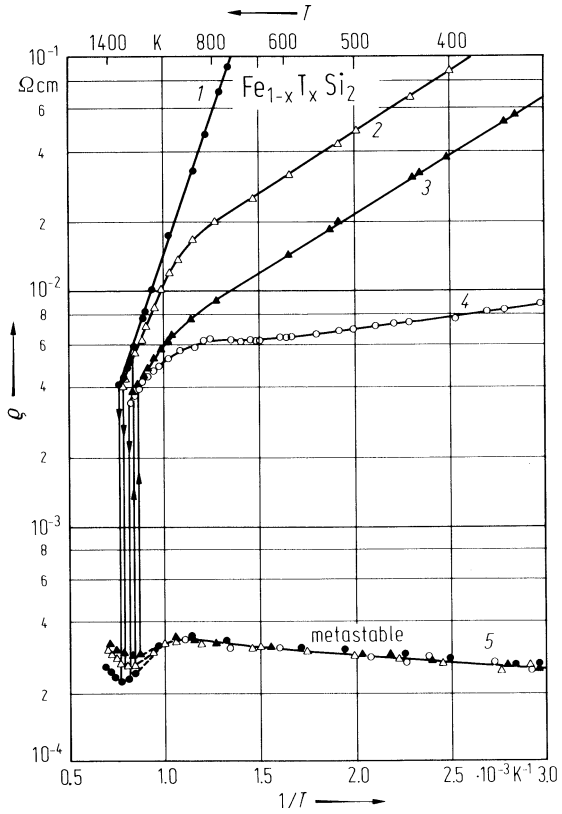

Fig. 5.

$Fe_{1-x}Mn_xSi_2$. Resistivity vs. reciprocal temperature in the intrinsic region for hot-pressed annealed samples [73N]. The solid curves represent the fitted calculated values.

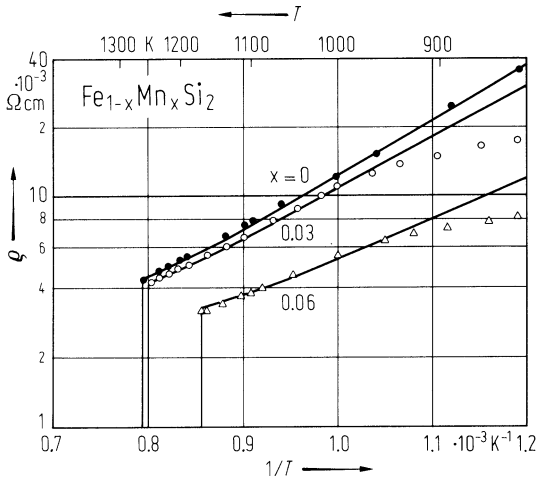

Fig. 6.

$Fe_{1-x}Co_xSi_2$. Hall coefficient and carrier concentration vs. reciprocal temperature [68B]. All samples n-type; prepared by sintering at 1453 K and annealing at 1153 K.

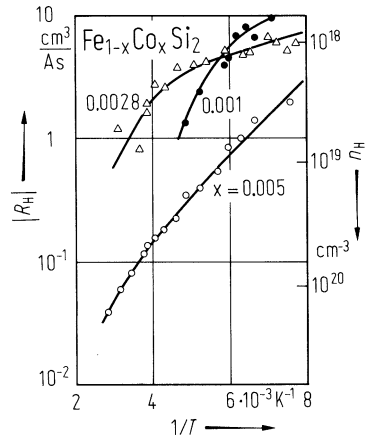

Fig. 7.

$FeSi_2$. Thermoelectric power vs. reciprocal temperature [64W]. Reference element: platinum. The three samples differed slightly in impurity content. The samples were prepared by rapidly freezing the melt in 3 mm silica capillaries (to ensure a fine dispersion of FeSi in the FeSi–α-$FeSi_2$ eutectic) and annealing at 1173 K. $|R_H| < 1$ $cm^3\ C^{-1}$. Unknown impurity content. Corrected absolute values for the intrinsic region are indicated by a dashed line.

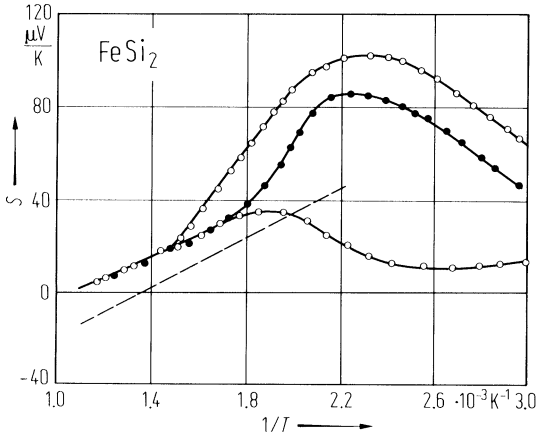

Fig. 8.

$FeSi_2$. Thermoelectric power vs. reciprocal temperature in the intrinsic and phase transition range for sintered material [70B].

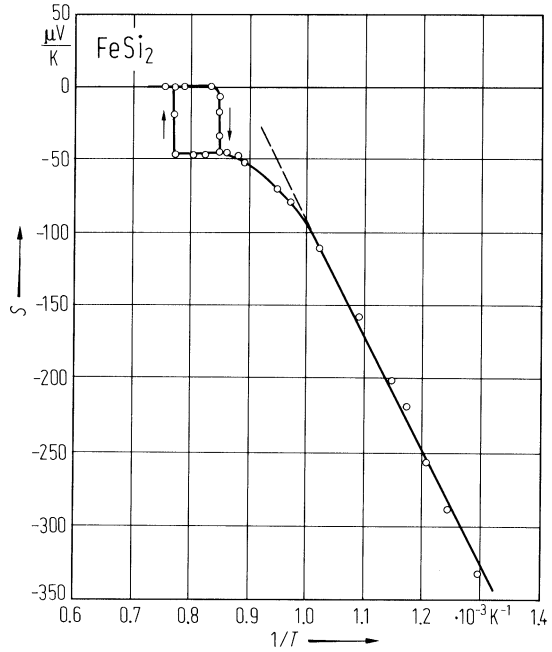

Fig. 9.

$Fe_{1-x}Co_xSi_2$ and $FeSi_{2-y}Al_y$. Thermoelectric power vs. temperature for quenched samples annealed at 1173K [64W]. *1*: x = 0.005, *2*: x = 0.01, *3*: x = 0.02, *4*: x = 0.03, *5*: x = 0.04. *6*: y = 0.02, *7*: y = 0.04, *8*: y = 0.05.

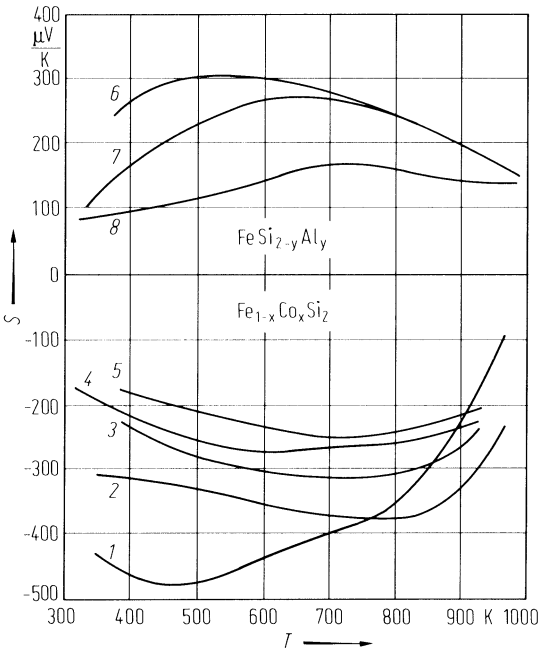

Fig. 10.

$Fe_{1-x}Co_xSi_2$. Thermoelectric power vs. temperature for weakly doped n-type samples [68B]. Samples sintered at 1453 K and annealed at 1153 K.

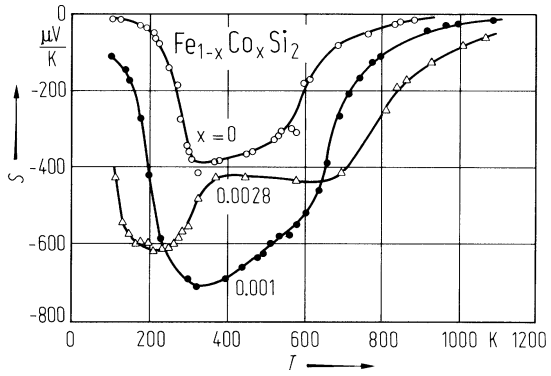

Fig. 11.

$Fe_{1-x}Co_xSi_2$. Thermoelectric power vs. temperature for heavily doped n-type samples [68B]. Samples sintered at 1453 K and annealed at 1153 K.

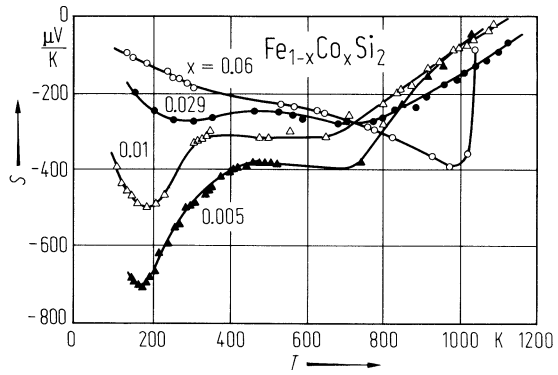

Fig. 12.

$FeSi_{2-y}Al_y$. Thermoelectric power vs. temperature for p-type samples [68B]. Samples sintered at 1453 K and annealed at 1153 K. Al loss due to evaporation during melting and sintering unknown.

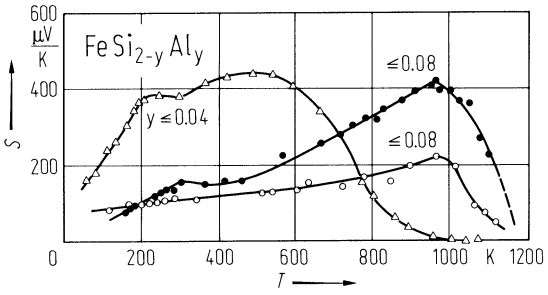

Fig. 13.

$Fe_{1-x}Mn_xSi_2$ and $Fe_{0.95}Co_{0.05}Si_2$. Thermoelectric power vs. temperature for hot-pressed and annealed samples [73N]. Heating and cooling transition directions are indicated by arrows. *1*: x = 0 (p-type), *2*: x = 0.03 (p-type), *3*: x = 0.06 (p-type), *4*: $Fe_{0.95}Co_{0.05}Si_2$ (n-type), *5*: metastable FeSi/$Fe_{\approx 0.8}Si_2$ mixture.

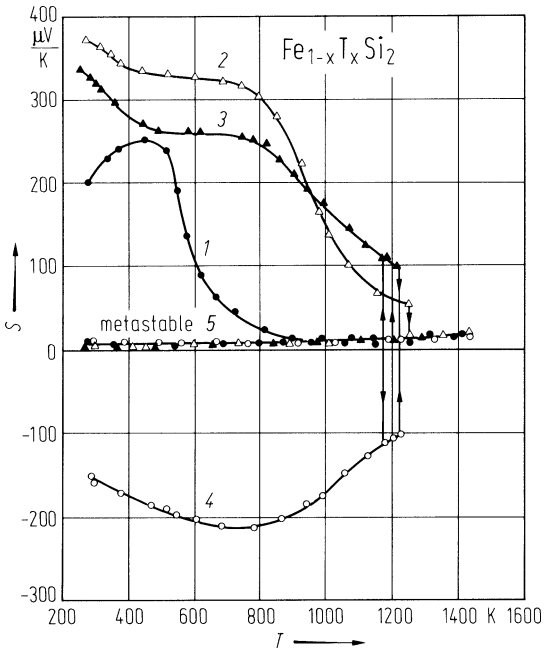

Fig. 14.

$Fe_{1-x}Co_xSi_{2-y}Al_y$. Thermal conductivity vs. temperature for sintered samples [73W]. Data of the metastable inhomogeneous high-temperature phase for comparison (Curve *5*). Curve *1*: x = 0, y = 0; *2*: x = 0, y = 0.04; *3*: x = 0.03, y = 0: *4*: x = 0.06. y = 0.

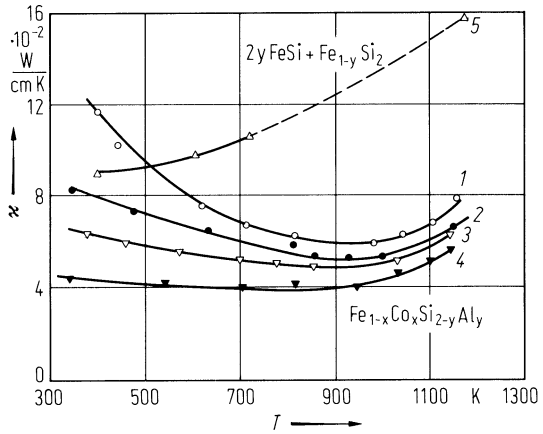

Fig. 15.

$Fe_{1-x}Co_xSi_2$. Thermal conductivity vs. temperature in a doubly-logarithmic scale; sintered samples [73W].

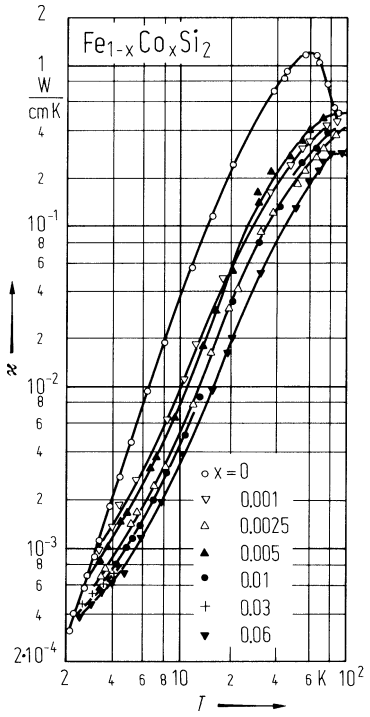

Fig. 16.

$FeSi_2$. Thermal resistivity vs. temperature for sintered samples [73W]. Curve *a* measured, *b* calculated with the formula of Price for the ambipolar part: $\kappa_{ambip.} = (k/e)^2 T\{\sigma_n\delta_n+\sigma_p\delta_p + (\sigma_n\sigma_p/\sigma)(((E_g(0)-\beta T)/kT)+\delta_n+\delta_p)^2\}$, where δ_n and δ_p are scattering parameters. Polar optical scattering with $\delta_n = \delta_p \approx 2.5$ was assumed. Since $\mu_n \approx \mu_p$ in $FeSi_2$, $\sigma_n \approx \sigma_p$ in the intrinsic range. Best fit (curve *b*) with $E_g(0) = 0.9$ eV and $\beta = 4.5\cdot10^{-4}$ eV K^{-1}. *c* lattice thermal resistivity. Electrical conductivity is also shown.

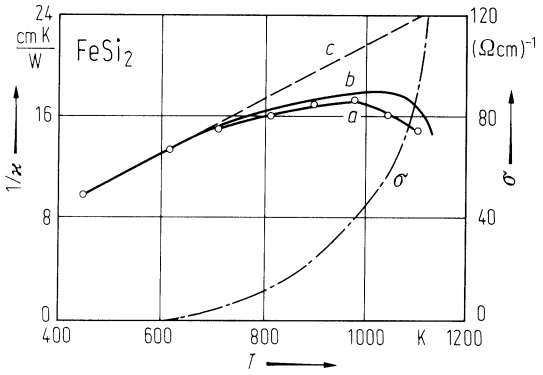

Fig. 17.

$FeSi_2$. Thermal conductivity vs. temperature in a doubly-logarithmic scale [73W]. Sintered samples. Curve *a*: undoped, *b*: $2.1 \cdot 10^{21}$ Al atoms/cm^3, *c*: $1.6 \cdot 10^{21}$ Co atoms/cm^3.

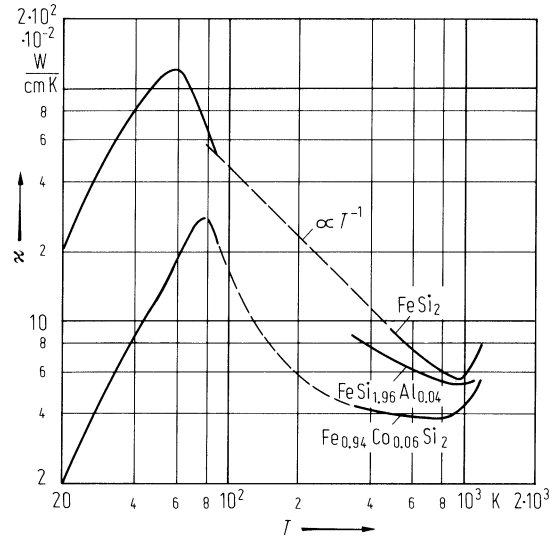

Fig. 18.

$Fe_{1-x}Mn_xSi_2$ and $Fe_{0.95}Co_{0.05}Si_2$. Hall mobility $\mu_H = R_H/\rho$ vs. reciprocal temperature in a doubly- logarithmic scale [73N]. Mn-doped samples: $\mu_{H,p}$; Co-doped sample: $\mu_{H,n}$; all samples hot-pressed at 1400 K and annealed at 1073 K.